

Magnetic Excitations in Polyoxometalate Clusters Observed by Inelastic Neutron Scattering: Evidence for Ferromagnetic Exchange Interactions and Spin Anisotropy in the Tetrameric Nickel(II) Cluster $[\text{Ni}_4(\text{H}_2\text{O})_2(\text{PW}_9\text{O}_{34})_2]^{10-}$ and Comparison with the Magnetic Properties

Juan M. Clemente-Juan,[†] Hanspeter Andres,[‡] Juan J. Borrás-Almenar,[†] Eugenio Coronado,^{*,†} Hans U. Güdel,^{*,‡} Michael Aebbersold,[‡] Gordon Kearly,[§] Herma Büttner,[§] and Markus Zolliker^{||}

Contribution from the Departamento de Química Inorgánica, Universidad de Valencia, C/ Dr. Moliner 50, 46100-Burjassot, Spain, Departement für Chemie und Biochemie, Universität Bern, Freiestrasse 3, 3000 Bern 9 Switzerland, Institut Laue Langevin, Avenue des Martyrs, B. P. 156, F-38042 Grenoble Cedex 9, France, and Laboratorium für Neutronenstreuung, ETH Zürich & PSI Villigen, 5232 Villigen PSI, Switzerland

Received January 20, 1999

Abstract: The ground-state properties of the tetranuclear Ni^{2+} cluster $[\text{Ni}_4(\text{H}_2\text{O})_2(\text{PW}_9\text{O}_{34})_2]^{10-}$ were investigated by combining magnetic susceptibility and magnetization measurements with a detailed inelastic neutron scattering (INS) study on a fully deuterated sample of $K_6\text{Na}_4[\text{Ni}_4(\text{H}_2\text{O})_2(\text{PW}_9\text{O}_{34})_2] \cdot 24\text{H}_2\text{O}$. The temperature dependence of the magnetic susceptibility indicates a ferromagnetic coupling of the four constituent Ni^{2+} ions ($s = 1$), and a low-temperature magnetization study provides the magnitude of the $S = 4$ ground-multiplet splitting due to the single-ion anisotropy of the Ni^{2+} ions. Besides a more direct and precise determination of the anisotropic $S = 4$ ground-multiplet splitting, INS enabled the determination of excited spin multiplets. The best fit to the experimental energy level diagram was obtained by an isotropic Spin Hamiltonian with the inclusion of axial single-ion anisotropy: $H = -2J(S_1S_3 + S_1S_4 + S_2S_3 + S_2S_4) - 2J'S_1S_2 + D(S_{z1}^2 + S_{z2}^2)$, where $J = 0.83$ meV, $J' = 0.39$ meV, $D = 0.47$ meV, and $D' = 0.60$ meV. Within this model the experimental intensities of the magnetic cluster excitations, their characteristic dependence on the scattering vector \mathbf{Q} , as well as the temperature dependence of the magnetic susceptibility and the magnetization properties are reproduced.

Introduction

Polyoxometalates are a rich class of inorganic compounds with a remarkable degree of molecular and electronic tunabilities that impact in disciplines as diverse as catalysis, medicine, and materials science.¹ An aspect of recent genesis and development in this area is that of the magnetism in these clusters. Two classes of polyoxometalates are relevant in this context: (1) The heteropoly complexes of W and Mo, as these diamagnetic frameworks can coordinate clusters of paramagnetic metal ions while keeping them well isolated from the neighboring magnetic clusters.² Therefore, they provide ideal models to study the exchange interactions in clusters of increasing nuclearities and definite topologies. In addition, they can be reversibly reduced to mixed-valence species (heteropoly “blues” and “browns”) by injection of a variable numbers of electrons, which are

delocalized over a significantly large number of centers of the heteropoly framework.³ (2) The polyoxovanadates, as they can be formed by large numbers of exchange-coupled $s = 1/2$ oxovanadium (IV) centers (14, 15, and 18), having, at the same time, the ability of being partially oxidized to give rise to mixed-valence clusters.⁴

Focusing on the heteropoly anions, until very recently the magnetic properties of these clusters have been only loosely investigated.⁵ The first work in this respect was reported by Baker et al.⁶ in 1972. These authors investigated the exchange-coupled pairs contained in a series of isomorphous complexes $[\text{M}'(\text{H}_2\text{O})\text{MW}_{11}\text{O}_{39}]^{n-}$ ($\text{M} = \text{Fe(III)}, \text{Co(II)}$; $\text{M}' = \text{Co(II)}, \text{Fe(III)}, \text{Co(III)}$), having the well-known Keggin structure. Recently the introduction of one or two delocalized electrons in these magnetic polyoxometalates allowed us to investigate the interplay of electron transfer and magnetic interactions at the molecular level.⁷ A systematic work on the magnetic properties

[†] Universidad de Valencia.

[‡] Universität Bern.

[§] Institut Laue Langevin.

^{||} Laboratorium für Neutronenstreuung.

(1) (a) An updated revision of the state-of-the-art in this burgeoning subarea of chemistry can be found in the special thematic issue of *Chem. Rev.* **1998**, *98*, 1–390. (b) Pope, M. T.; Müller, A. *Polyoxometalates: From Platonic Solids to Anti-Retroviral Activity*; Kluwer Academic Publishers: Dordrecht, The Netherlands, 1994.

(2) Coronado, E.; Gómez-García, C. J. *Comments Inorg. Chem.* **1995**, *17*, 255.

(3) Pope, M. T. *Heteropoly and Isopoly Oxometalates*; Springer-Verlag: Berlin, Germany, 1983.

(4) Müller, A.; Peters, F.; Pope, M. T.; Gatteschi, D. *Chem. Rev.* **1998**, *98*, 239.

(5) For a review on the magnetism of these clusters see Clemente-Juan, J. M.; Coronado, E. *Coord. Chem. Rev.*, in press.

(6) (a) Baker, L. C. W.; Baker, V. E. S.; Wasfi, S. H.; Candela, G. A.; Kahn, A. H. *J. Am. Chem. Soc.* **1972**, *94*, 5499. (b) Baker, L. C. W.; Baker, V. E. S.; Wasfi, S. H.; Candela, G. A.; Kahn, A. H. *J. Chem. Phys.* **1972**, *56*, 4917.

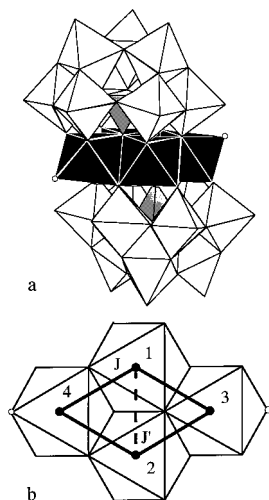


Figure 1. (a) Polyhedral representation of the $[\text{Ni}_4(\text{PW}_9\text{O}_{34})_2(\text{D}_2\text{O})_2]^{10-}$ anion. (b) Exchange network of the M_4O_{16} cluster showing the two different exchange pathways J and J' .

of higher nuclearity heteropoly anions was initiated in 1990 on the series $[\text{M}_4(\text{H}_2\text{O})_2(\text{PW}_9\text{O}_{34})_2]^{10-}$ ($\text{M} = \text{Mn}(\text{II}), \text{Fe}(\text{II}), \text{Co}(\text{II}), \text{Ni}(\text{II}), \text{Cu}(\text{II})$).⁸ In this extensive series of compounds first reported by Tourné et al.⁹ and subsequently characterized by Finke et al.¹⁰ and Weakley et al.,¹¹ a tetranuclear magnetic cluster M_4O_{16} is encapsulated by two heptadentate tungstophosphate ligands $[\text{PW}_9\text{O}_{34}]^{9-}$ (see Figure 1a). This diamagnetic anion is the trivacant lacunary fragment that results from the removal of a triad of tungsten sites from the Keggin anion $[\text{PW}_{12}\text{O}_{40}]^{3-}$. A related series of tetranuclear magnetic clusters is that based upon the heptadentate ligand $[\text{P}_2\text{W}_{15}\text{O}_{56}]^{12-}$, which is the trivacant lacunary fragment of the Dawson-Wells anion $[\text{P}_2\text{W}_{18}\text{O}_{62}]^{6-}$.¹² In all of these clusters the rigidity of the polyoxometalate framework imposes a rhomb-like geometry for the magnetic cluster in such a way that the $\text{M}-\text{O}-\text{M}$ angles are close to 90° , thus favoring ferromagnetic coupling and stabilizing large spin ground states. In addition, an important feature of this chemistry is that it allows the formation of large clusters using preformed building blocks. Thus, by reaction of the $[\text{PW}_9\text{O}_{34}]^{9-}$ ligand with $\text{M}(\text{II}) = \text{Ni}$ and Co , the magnetic nuclearity of the heteropoly complex can be increased from 4 to 9.^{2,13}

The aim of the present and following paper¹⁴ is to obtain detailed information on the exchange interactions in the tetranuclear ferromagnetic clusters of $\text{Ni}(\text{II})$ and $\text{Co}(\text{II})$. Usually this

kind of information is derived from the analysis of the temperature dependence of the magnetic susceptibility. This indirect method requires first the choice of a model to fit the experimental data and leads subsequently to values of the exchange parameters and of the other relevant magnetic parameters. The danger in this procedure lies in the low information content of the susceptibility data, which often does not allow discrimination between physically different models. This is particularly dramatic in the tetrameric clusters discussed here due to both the rhomb-like topology of the exchange interactions (see Figure 1b) and the nature of the interacting metal ions. Thus, it has been found that, in these cases, susceptibility is little sensitive to the exchange parameter of the diagonal of the rhomb J' and to the exchange anisotropy.⁶

Here we will use a more direct approach to obtain the low-lying energy levels of the cluster and thus the relevant magnetic parameters. By using the spectroscopic technique of inelastic neutron scattering (INS), we will determine the experimental energy-level diagram independent of any theoretical model. In a second step we will reproduce this energy-level pattern by the eigenvalues of an appropriate Spin Hamiltonian. In a final step we will check if the differential neutron cross-section, calculated on the basis of the corresponding eigenfunctions, is able to reproduce the experimental intensities of the magnetic cluster excitations as well as their characteristic dependence on the scattering vector \vec{Q} . This will be an additional proof of the validity of the proposed model.

INS has proved its capability in the study of clusters of transition metal ions and rare earths.¹⁵ However, few examples have been studied so far, most of them dimers or isotropic exchange systems with higher nuclearity. To notice is a $\text{Ni}(\text{II})$ dimer in which inclusion of single anisotropy was taken into account.¹⁶ Anisotropy was also considered in various rare-earth dimer systems as well as in mixed rare-earth/transition-metal dimers.¹⁷ As higher nuclearity clusters we should mention a Cr_4^{3+} cluster with rhomb-like geometry¹⁸ and a $\text{Ti}^{2+}(\text{Mn}^{2+})_6$ cluster,¹⁹ as well as the dodonuclear $\text{Mn}_{12}^{3+/4+}$ acetate cluster.²⁰ This last example represents the largest spin cluster treated so far by INS, although INS was used in this case to obtain information on the ZFS of the ground spin state $S = 10$, only. We will show here that this technique can also be used to study the often more complex high-nuclearity magnetic clusters furnished by polyoxometalate chemistry. In these cases the additional information obtained from INS becomes invaluable.

Experimental Section

Synthesis. $\text{K}_6\text{Na}_4[\text{Ni}_4(\text{H}_2\text{O})_2(\text{PW}_9\text{O}_{34})_2] \cdot 24\text{H}_2\text{O}$ was prepared according to the following method:^{13b} To 100 mL of an aqueous solution containing 33 g (100 mmol) of $\text{Na}_2\text{WO}_4 \cdot 2\text{H}_2\text{O}$ and 1.57 g (11 mmol)

(7) (a) Casañ-Pastor N.; Baker L. C. W. *J. Am. Chem. Soc.* **1992**, *114*, 10384. (b) Casañ-Pastor N.; Baker L. C. W. in ref 1b; p 203.

(8) (a) Gómez-García, C. J.; Casañ-Pastor, N.; Coronado, E.; Baker, L. C. K.; Pourroy, G. *J. Appl. Phys.* **1990**, *67*, 5995. (b) Casañ-Pastor, N.; Bas-Serra, J.; Coronado, E.; Pourroy, G.; Baker, L. C. K. *J. Am. Chem. Soc.* **1992**, *114*, 10380. (c) Gómez-García, C. J.; Coronado, E.; Borrás-Almenar, J. J. *Inorg. Chem.* **1992**, *31*, 1669. (d) Gómez-García, C. J.; Coronado, E.; Gómez-Romero, P.; Casañ-Pastor, N. *Inorg. Chem.* **1993**, *32*, 3378.

(9) Evans, H. T.; Tourné, C. M.; Tourné, G. T.; Weakley, T. J. R. *J. Chem. Soc., Dalton Trans.* **1986**, 2699.

(10) Finke, R. G.; Droeger, M. W.; Domaille, P. J. *Inorg. Chem.* **1987**, *26*, 3886.

(11) Weakley, T. J. R.; Finke, R. G. *Inorg. Chem.* **1990**, *29*, 1235.

(12) Gómez-García, C. J.; Borrás-Almenar, J. J.; Coronado, E.; Ouahab, L. *Inorg. Chem.* **1994**, *33*, 4016.

(13) (a) Galán-Mascarós, J. R.; Gómez-García, J. C.; Borrás-Almenar, J. J.; Coronado, E. *Adv. Mater.* **1994**, *6*, 221. (b) Clemente-Juan, J. M.; Coronado, E.; Galán-Mascarós, J. R.; Gómez-García, C. J. *Inorg. Chem.*, in press.

(14) Andres, H.; Clemente-Juan, J. M.; Aebersold, M.; Güdel, H. U.; Coronado, E.; Büttner, H.; Kearly, G.; Melero J.; Burriel, R. *J. Am. Chem. Soc.* **1999**, *121*, 10028–10034.

(15) (a) Güdel, H. U.; Furrer, A. *Mol. Phys.* **1977**, *5*, 1335. (b) Güdel, H. U. in *Molecular Magnetism: From Molecular Assemblies to the devices*; Coronado, E., Delhaès, P., Gatteschi, D., Miller, J. S., Eds.; Kluwer Academic Press: Dordrecht, The Netherlands, 1996; NATO ASI Series E, Vol. 321, pp 229–242.

(16) Stebler, A.; Güdel, H. U.; Furrer, A.; Kjems, J. K. *Inorg. Chem.* **1982**, *21*, 380.

(17) (a) Güdel, H. U.; Furrer, A.; Blank, H. *Inorg. Chem.* **1990**, *29*, 4081. (b) Furrer, A.; Güdel, H. U.; Krausz, E. R.; Blank, H. *Phys. Rev. Lett.* **1990**, *64*, 68. (c) Aebersold, M. A.; Güdel, H. U.; Hauser, A.; Furrer, A.; Blank, H.; Kahn, R. *Phys. Rev. B* **1993**, *48*, 12723. (d) Güdel, H. U. *Neutron News* **1996**, *73*, 24.

(18) (a) Furrer, A.; Güdel, H. U.; Hauser, U. *J. Appl. Phys.* **1979**, *50*, 2043. (b) Güdel, H. U.; Hauser, U.; Furrer, A. *Inorg. Chem.* **1979**, *18*, 2730.

(19) Aebersold, M.; Blank, H.; Briat, B.; Furrer, A.; Güdel, H. U. *Inorg. Chem.* **1991**, *30*, 3280.

(20) Hennion, M.; Pardi, L.; Mirebeau, I.; Suard, E.; Sessoli, R.; Caneschi, A. *Phys. Rev. B* **1997**, *56*, 8819.

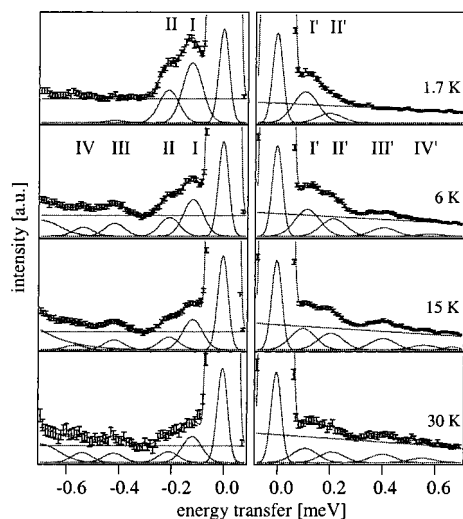


Figure 2. Neutron-energy loss and gain spectra of the polycrystalline sample $\text{K}_6\text{Na}_4[\text{Ni}_4(\text{D}_2\text{O})_2(\text{PW}_9\text{O}_{34})_2] \cdot 24\text{D}_2\text{O}$ measured on IN5 with an incident neutron wavelength of 6.5 Å at the temperatures 1.7, 6, 15, and 30 K with inclusion of least-squares fits as solid lines.

of Na_2HPO_4 (pH adjusted to 7.1 with acetic acid) was added a solution of 5.53 g (22 mmol) of Ni(II) acetate in 50 mL H_2O . The resulting yellow solution (pH = 6.9) was refluxed for 2 h and hot filtered, and then 4 g of potassium acetate was added before allowing the solution to cool to room temperature. After several hours, a mixture of chunky small yellow crystals and powder is obtained. The deuterated complex was obtained after two recrystallizations in D_2O . All of the neutron scattering measurements were performed on this deuterated sample sealed under helium in a cylindrical aluminum container (15 mm diameter and 55 mm length) suitable for INS experiments.

Inelastic Neutron Scattering. All experiments were carried out at the Institut Laue-Langevin (ILL) in Grenoble. Three different spectrometers were used: the time-of-flight (TOF) spectrometers IN5 and IN6 and the triple-axis (3ax) spectrometer IN3. The measurements on IN6 were performed at temperatures of 1.7, 10, and 30 K with incident neutron wavelengths of 4.1 and 5.9 Å. On IN5 the temperatures were 1.7, 6, 15, and 30 K and the incident neutron wavelength was 6.5 Å. In both cases a background spectrum using an empty aluminum container of the same size was subtracted and the detectors were calibrated by means of a spectrum of vanadium metal. The time-of-flight to energy conversion and the data reduction were done with the standard program INX at the ILL. INS spectra on IN3 were performed with thermal neutrons of 2.44 Å at temperatures of 10 and 30 K. The axes of the spectrometer were chosen to scan the neutron-energy loss region at constant Q values. The data treatment involved the subtraction of a constant background. Further data treatment was done using the commercial program IGOR (Wavemetrics).

Magnetic Measurements. Variable-temperature susceptibility measurements were carried out in the temperature range 2–300 K at a magnetic field of 0.1 T using a magnetometer (Quantum Design MPMS-XL-5) equipped with a SQUID sensor. Isothermal magnetization measurements as a function of the external magnetic field were performed up to 5 T at 2 K. The magnetization was also measured as a function of the temperature at different fields (1, 1.5, 2, 2.5, 3, and 4 T).

Results

Inelastic Neutron Scattering. In Figure 2 we report the INS spectra of a polycrystalline sample of $\text{K}_6\text{Na}_4[\text{Ni}_4(\text{D}_2\text{O})_2(\text{PW}_9\text{O}_{34})_2] \cdot 24\text{D}_2\text{O}$ at temperatures $T = 1.7, 6, 15,$ and 30 K. The incident neutron wavelength of 6.5 Å on IN5 allowed us to cover the energy-transfer range from -1.2 (neutron-energy

Table 1. Observed and Calculated INS Intensities for the TOF Experiment^a

label	energy [meV]		1.7 K	6 K	15 K	30 K
I	-0.11	calcd	1	0.58	0.37	0.22
		exp.	1 ± 0.02	0.63 ± 0.02	0.50 ± 0.02	0.39 ± 0.04
II	-0.21	calcd	0.54	0.44	0.31	0.19
		exp.	0.54 ± 0.02	0.31 ± 0.02	0.22 ± 0.02	0.22 ± 0.04
III	-0.41	calcd	0.10	0.21	0.20	0.13
		exp.	0.03 ± 0.02	0.22 ± 0.02	0.18 ± 0.02	0.15 ± 0.04
IV	-0.55	calcd	0	0.06	0.08	0.07
		exp.	0	0.10 ± 0.02	0.09 ± 0.03	0.08 ± 0.05
I'	0.11	calcd	0.61	0.49	0.34	0.21
		exp.	0.44 ± 0.01	0.38 ± 0.02	0.30 ± 0.02	0.20 ± 0.02
II'	0.21	calcd	0.13	0.27	0.26	0.17
		exp.	0.13 ± 0.01	0.25 ± 0.02	0.24 ± 0.02	0.15 ± 0.02
III'	0.41	calcd	0	0.10	0.15	0.11
		exp.	0	0.12 ± 0.02	0.16 ± 0.02	0.12 ± 0.02
IV'	0.55	calcd	0	0.02	0.06	0.05
		exp.	0	0.03 ± 0.02	0.06 ± 0.02	0.06 ± 0.02
V	-3.50	calcd	0.59			0.32
		exp.	0.40 ± 0.05			0.19 ± 0.05

^a The calculation is based on the Spin Hamiltonian in eq 1 with the parameter set given in eq 2. The experimental values are the total of all Q values.

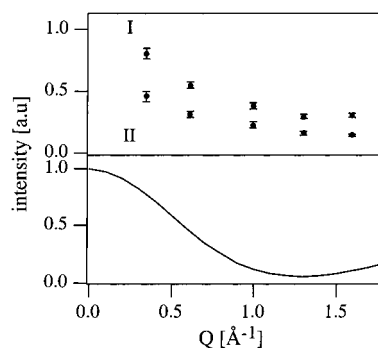


Figure 3. (Top) Intensity of the transitions I and II as a function of the scattering vector Q as obtained from least-squares fits of the 6.5 Å spectrum at 1.7 K. (Bottom) Calculated intensity behavior of the transitions I–IV on the basis of the coupled cluster wave functions given in Table 2. The data and the calculated curves are scaled to a value of 1 at $Q = 0$ for transition I.

loss) to 1.2 meV²¹ (neutron-energy gain) with a resolution of 50 μeV . The experimental data were fit assuming a linear background and Gaussians with equal line widths to describe the inelastic transitions. Additionally, on the neutron-energy loss side below -0.5 meV, we introduced a polynomial expression to reproduce the nonlinear increase of the background intensity. Four transitions centered at 0.11, 0.21, 0.41, and 0.55 meV, labeled I, II, III, and IV, respectively, are observed on the neutron-energy loss side between 1.7 and 30 K. Primed labels of the corresponding transitions are used on the gain side. In Table 1 we list the positions and intensities of the various transitions obtained from the least-squares fits in Figure 2 at the experimental temperatures. The good statistics of the 1.7 K spectrum enabled us to study the behavior of the scattering intensities of transitions I–IV as a function of the scattering vector Q . They all show a continuous drop of the intensity down to a minimum around 1.4 \AA^{-1} , as depicted for transitions I and II in Figure 3.

The neutron-energy loss spectra measured on IN6 at 1.7 and 30 K are depicted in Figure 4. An incident neutron wavelength of 4.1 Å covers the energy-transfer range down to -3.8 meV

(21) The common energy unit in neutron scattering is $1 \text{ meV} = 8.0655 \text{ cm}^{-1}$.

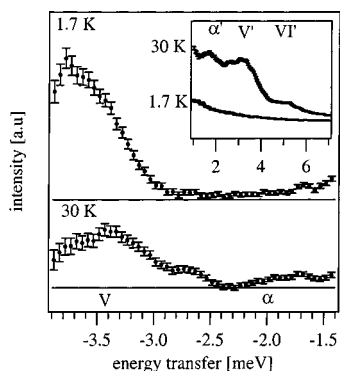


Figure 4. Neutron-energy loss and gain spectra of the polycrystalline sample $\text{K}_6\text{Na}_4[\text{Ni}_4(\text{D}_2\text{O})_2(\text{PW}_9\text{O}_{34})_2]\cdot 24\text{D}_2\text{O}$ measured on IN6 with an incident neutron wavelength of 4.1 Å at the temperatures 1.7 and 30 K.

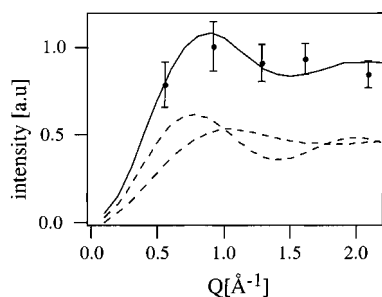


Figure 5. Total intensity of the band V in Figure 4 as a function of the scattering vector \vec{Q} at 30 K. The calculated intensity was obtained on the basis of the coupled cluster wave functions given in Table 2. Dashed lines represent the two types of Q dependencies which contribute to the band behavior.

on the loss side with a resolution of 170 μeV . A spurious peak at -0.8 meV, most probably due to a Bragg reflection of the aluminum shield in the cryostat, masks the information between -1 and 0 meV. The spectrum at 1.7 K is dominated by a complex and broad band centered at 3.6 meV, labeled V as seen by inspection of Figure 4. Its irregular shape and large width, compared with the instrumental resolution and with similar transitions observed under the same experimental conditions in the analogous cobalt cluster,¹⁴ indicate a convolution of several transitions. When the temperature is increased to 30 K, the shape of band V changes markedly and its center shifts toward lower transfer energy. New hot bands appear around 2.0 and 2.7 meV; the most intense one is labeled α , corresponding to transitions from excited spin multiplets. Band V is best fit with a constant background and with convoluted Gaussians of equal line width, and the resulting intensity is included in Table 1. The total intensity behavior of band V versus scattering vector \vec{Q} is depicted in Figure 5. We note the very different Q dependence in comparison with transition I–IV (compare Figure 3). The corresponding energy gain spectra at 4.1 Å are shown in the inset of Figure 4. At 1.7 K no inelastic transition occurs in the experimental range 0–7 meV, whereas at 30 K one observes the bands V' and α' and a new band around 5.1 meV labeled VI' .

The use of thermal neutrons with an incident neutron wavelength of 2.44 Å expands the energy-transfer range on the neutron-energy loss side to -9 meV. Due to the presence of phonon scattering below -6 meV, whose intensity rises with Q^2 , we only consider the spectrum obtained at $Q = 1.0$ Å⁻¹ as depicted in Figure 6. One observes in addition to the band V two new bands centered at -5.1 and -7 meV (labeled VI and VII, respectively). Due to the underlying phonon intensity, it is

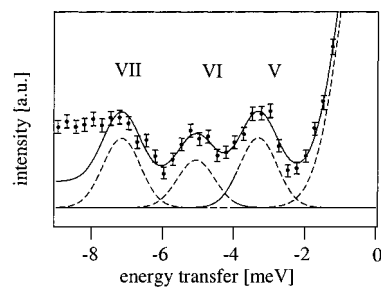


Figure 6. Neutron-energy loss spectra of the polycrystalline sample $\text{K}_6\text{Na}_4[\text{Ni}_4(\text{D}_2\text{O})_2(\text{PW}_9\text{O}_{34})_2]\cdot 24\text{D}_2\text{O}$ measured on IN3 with an incident neutron wavelength of 2.44 Å at $T = 10$ K and $Q = 1.0$ Å⁻¹.

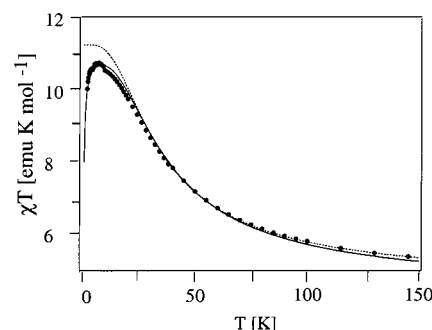


Figure 7. Thermal dependence of the product χT for $\text{K}_6\text{Na}_4[\text{Ni}_4(\text{D}_2\text{O})_2(\text{PW}_9\text{O}_{34})_2]\cdot 24\text{D}_2\text{O}$ (filled circles) and the best fit to the experimental data obtained using the exchange and ZFS parameters in eq 2 and $g = 2.08$ (solid line). The theoretical behavior of a fully isotropic ferromagnetic Ni4 cluster is included as a dotted line.

difficult to estimate the position and intensity of band VII. With the linear background chosen in Figure 6, its intensity is clearly overestimated and will therefore not be used in the analysis.

Magnetic Measurements. The magnetic susceptibility data of the deuterated sample are reported as a plot of χT versus temperature in Figure 7. Within the experimental error they agree with those previously reported for the nondeuterated sample.^{13b} Magnetization measurements can be used to get complementary information on the nature of the ground spin multiplet, as well as on its splitting due to the single-ion anisotropy. The isothermal magnetization curve as a function of the applied magnetic field at 2 K is plotted in Figure 8a. These measurements are complemented with magnetization data at different temperatures and different fields. These are reported as a plot of the magnetization versus the inverse of the temperature for magnetic fields between 1 and 4 T in Figure 8b.

Analysis and Discussion

General Considerations on the Ni(II) Tetramer. In the $[\text{M}_4(\text{H}_2\text{O})_2(\text{PW}_9\text{O}_{34})_2]^{10-}$ series, the structure of the magnetic cluster M_4O_{16} consists of four coplanar $\text{M}^{\text{II}}\text{O}_6$ octahedra sharing edges with a rhomb-like shape, as shown in Figure 1b. Such a geometry leads to two types of pairwise nearest-neighbor exchange interactions indicated by the two parameters J and J' . In addition there is the possibility of a smaller next-nearest-neighbor interaction across the long diagonal. Furthermore it is to be noted that in the cluster two distinct metal sites can be distinguished, as the M^{II} ions of the long diagonal of the rhomb (3 and 4 in Figure 1b) complete the octahedral coordination with two water molecules. These latter exhibit a larger axial distortion. In the particular case of Ni(II), this should result in two different single-ion zero-field splitting (ZFS) parameters D and D' for the pairs of sites 1/2 and 3/4, respectively. On the

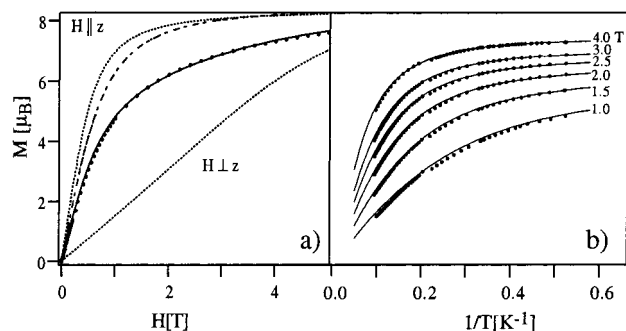


Figure 8. (a) Magnetization vs magnetic field for $\text{K}_6\text{Na}_4[\text{Ni}_4(\text{D}_2\text{O})_2(\text{PW}_9\text{O}_{34})_2] \cdot 24\text{D}_2\text{O}$ at 2 K (filled circles). Comparison with the Brillouin function of a $S = 4$ spin state (dashed-dotted line) and with the magnetization calculated using the exchange and ZFS parameters in eq 2 and $g = 2.08$ (solid line). This curve has been obtained by averaging the magnetization calculated for different orientations of the field with respect to the cluster axis, see the dashed curves for $H \perp z$ and $H \parallel z$. (b) Magnetization curve vs the inverse of the temperature for $\text{K}_6\text{Na}_4[\text{Ni}_4(\text{D}_2\text{O})_2(\text{PW}_9\text{O}_{34})_2] \cdot 24\text{D}_2\text{O}$ at different fields (filled circles). The solid line represents the calculated behavior using the exchange parameters from eq 2, $\bar{D} = 0.543$ meV and $g = 2.08$.

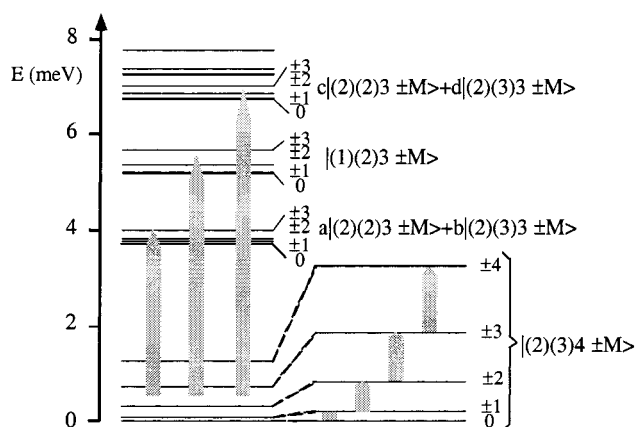


Figure 9. Experimental energy-level diagram derived from the INS experiments with the main contributions to the eigenfunctions. The arrows indicate the experimental transitions.

other hand, since the single-ion ground state of Ni(II) is an orbital singlet (3A_2 term), isotropic exchange interactions can be expected. Accordingly, the effective Spin Hamiltonian describing this tetramer is given by

$$H = -2J(S_1S_3 + S_1S_4 + S_2S_3 + S_2S_4) - 2J'S_1S_2 + D(S_{z1}^2 + S_{z2}^2) + D'(S_{z3}^2 + S_{z4}^2) \quad (1)$$

Previous magnetic susceptibility measurements^{13b} were used to roughly determine the exchange parameters J and J' in this cluster, with J in the range 0.78–0.88 meV and J' in the range 0–0.6 meV, respectively. The averaged ZFS parameter $\bar{D} = (D + D')/2$ lies in the range 0.25–0.63 meV. As we can see from the above values, the information content of the magnetic susceptibility data was insufficient for a reliable evaluation of all the relevant parameters involved in the Spin Hamiltonian in eq 1.

Analysis of the INS Spectra. On the basis of the results obtained from the INS spectra in Figures 2, 4, and 6, it is possible to derive an experimental energy-level diagram as depicted in Figure 9. It consists of a ground-state multiplet, further split into five components due to the single-ion anisotropy, and three excited multiplets centered at 3.6, 5.1, and 7.0 meV. Observed experimental transitions are shown as arrows.

Table 2. Experimental and Calculated Energy Levels with Corresponding Wavefunctions Expanded in the $|S_{12}(S_{123})SM\rangle$ Basis Obtained by Applying the Spin Hamiltonian in Eq 1 with the Parameter Set in Eq 2

experimental energy [meV]	calculated energy [meV]	main contributions to the functions $ S_{12}(S_{123})SM\rangle$
0	0	0.997 $ (2)(3)4 0\rangle$
0.11 ± 0.01	0.09	0.997 $ (2)(3)4 \pm 1\rangle$
0.32 ± 0.01	0.33	0.999 $ (2)(3)4 \pm 2\rangle$
0.73 ± 0.02	0.73	1.000 $ (2)(3)4 \pm 3\rangle$
1.28 ± 0.02	1.27	1.000 $ (2)(3)4 \pm 4\rangle$
band centered at 3.6	3.75	$-0.576 (2)(2)3 0\rangle + 0.815 (2)(3)3 0\rangle$
	3.76	$\mp 0.576 (2)(2)3 \pm 1\rangle \pm 0.813 (2)(3)3 \pm 1\rangle$
	3.82	$-0.575 (2)(2)3 \pm 2\rangle + 0.813 (2)(3)3 \pm 2\rangle$
	3.98	$\mp 0.577 (2)(2)3 \pm 3\rangle \pm 0.816 (2)(3)3 \pm 3\rangle$
band centered at 5.1	5.17	$ (1)(2)3 0\rangle$
	5.20	$\mp 0.990 (1)(2)3 \pm 1\rangle$
	5.37	$0.996 (1)(2)3 \pm 2\rangle$
	5.66	$ (1)(2)3 \pm 3\rangle$
band centered at 7.0	from 6.76 to 9.06	linear combinations of $ (2)(2)3 \pm M\rangle$, $ (2)(3)3 \pm M\rangle$, $ (2)(1)2 \pm M\rangle$, $ (2)(2)2 \pm M\rangle$ and $ (2)(3)2 \pm M\rangle$

The eigenvalues of the Spin Hamiltonian in eq 1 have been calculated by using the formalism developed by some of us.²² This formalism is based on the successive use of the Irreducible Tensor Operator techniques, which allow us to take fully into account all kinds of magnetic exchange interactions between the metal ions comprised in clusters of arbitrary nuclearity and spin values, as well as the single-ion anisotropic terms. The best fit to the experimental energy-level diagram was obtained with the following set of parameters:

$$J = 0.83 \text{ meV}, \quad J' = 0.39 \text{ meV}, \quad D = 0.47 \text{ meV}, \quad \text{and } D' = 0.60 \text{ meV} \quad (2)$$

A comparison of the calculated and observed energies is given in Table 2, and the overall agreement is excellent. Due to the single-ion anisotropy, the operator in eq 1 does not commute with \hat{S}^2 , the total spin of the cluster. Thus, the eigenfunctions are linear combinations of the $|S_{12}(S_{123})SM\rangle$ basis set functions, where S_{12} and S_{123} are intermediate spins defined as

$$S_1 + S_2 = S_{12}, \quad S_{12} + S_3 = S_{123}, \quad S_{123} + S_4 = S \quad (3)$$

The only valid quantum number for describing the cluster wave functions is M , as seen in Table 2. It is important to notice that the $S = 4$ multiplet splitting depends only on the average value of the single-ion anisotropy \bar{D} . Information on the individual single-ion anisotropies D and D' is accessible from the splitting of the excited $S = 3$ multiplets. As expected, a larger value is obtained for the parameter associated with the hydrated site D' . The two exchange parameters J and J' are determined by the energy differences of the $S = 4$ multiplet to the excited $S = 3$ multiplets. We can test the quality of the wave functions and thus the validity of the model by computing relative INS intensities and comparing them with the experimental values. We make use of the formalism developed in ref 22 which is of general validity. The relevant cross section formula for a transition between two basis functions $|S_{12}(S_{123})SM\rangle \rightarrow |(S'_{12})(S'_{123})S'M'\rangle$ is given by

(22) Borrás-Almenar, J. J.; Clemente-Juan, J. M.; Coronado, E.; Tsukerblat, B. S. *Inorg. Chem.*, in press.

$$\frac{\partial^2 \sigma}{\partial \Omega \partial \omega} = A \exp \left\{ - \frac{E(|(S_{12})(S_{123})SM\rangle)}{kT} \right\} \sum_{\alpha, \beta} \left(\delta_{\alpha\beta} - \frac{Q_\alpha Q_\beta}{Q^2} \right) \sum_{m, n} F_m^*(\vec{Q}) F_n(\vec{Q}) \exp\{i\vec{Q}(\vec{R}_m - \vec{R}_n)\} \times \langle (S_{12})(S_{123})SM | \hat{S}_m^\alpha | (S'_{12})(S'_{123})S'M' \rangle \times \langle (S'_{12})(S'_{123})S'M' | \hat{S}_n^\beta | (S_{12})(S_{123})SM \rangle \times \delta(\hbar\omega + E(|(S_{12})(S_{123})SM\rangle) - E(|(S'_{12})(S'_{123})S'M'\rangle)) \quad (4)$$

where $\alpha, \beta = x, y, z$; m and n number the Ni^{2+} ions within the cluster; $F_m(\vec{Q})$ is the magnetic form factor of Ni^{2+} ; and \vec{R}_m and \vec{R}_n are the position vectors of the Ni^{2+} ions in the cluster. The quantity A is composed of a constant and the Debye–Waller factor as follows:

$$A = \frac{\gamma e^2 k'}{m_e c^2 k} \exp(-2W)$$

Of particular relevance in eq 4 are the matrix elements of the form $\langle (S_{12})(S_{123})SM | \hat{S}_m^\alpha | (S'_{12})(S'_{123})S'M' \rangle$ and the so-called interference factor $\exp\{i\vec{Q}(\vec{R}_m - \vec{R}_n)\}$. The latter leads to a modulation of the INS intensities reflecting the nearest-neighbor Ni^{2+} – Ni^{2+} interactions. The matrix elements are characterized by coupled cluster wave functions and spin operators acting on individual spins. They are best evaluated by using tensor operator techniques, see ref 22.

The following selection rules are easily derived from these matrix elements

$$\Delta S_{12}, \Delta S_{123}, \Delta S, \text{ and } \Delta M = 0, \pm 1 \quad (5)$$

After proper integration over the measured Q range, we obtain the calculated relative intensities for transitions I–V given in Table 1. For transition I at elevated temperatures, we note a large difference between the experimental and calculated values. We attribute this to overlap with coinciding hot transitions originating in the excited multiplets, which are significantly populated at higher temperatures. In the following we will first discuss the low-energy INS transitions within the $S = 4$ multiplet, which define the zero-field splitting. The following paragraph is then devoted to the higher-energy transitions between the S multiplets.

Magnetic Transitions within the Ground Spin Multiplet $S = 4$. The ground spin multiplet is split into five levels with ΔM values ranging from 0 to 4. On the basis of the selection rule $\pm M = \pm 1$, we expect four magnetic transitions within this multiplet, in excellent agreement with the observed bands I–IV in Figure 2. The temperature dependence of the intensity and the position of these four transitions indicate that the ground level corresponds to $M = 0$ and the excited levels are successively $M = \pm 1, \pm 2, \pm 3$, and ± 4 . This unambiguously demonstrates that the ZFS parameter associated to each $\text{Ni}(\text{II})$ ion is positive. The zero-field splitting leads to energy intervals between adjacent levels of 1, 3, 5, and 7 in ground-state D_{cluster} units. For a pure $S = 4$ ground-state, the D_{cluster} can be expressed in terms of the individual ZFS parameters D and D' as follows:

$$D_{\text{cluster}} = \frac{(D + D')}{14} \quad (6)$$

The small deviations of the observed positions from this pattern are due to some admixing of the $S = 0$ and 2 multiplets. The

values for D and D' are given in eq 2. In the analysis we neglect a rhombic term in the ZFS Spin Hamiltonian of the Ni^{2+} centers since their actual point symmetry is not axial. Inclusion of a rhombic term improves the fit of the energy pattern but does not reproduce the temperature dependence of the INS intensities. The allowed $\Delta M = \pm 1$ transitions almost exclusively involve two levels with the same intermediate and total spin quantum numbers as seen in Table 2. Thus they have the same interference factors in the differential neutron cross section in eq 4 which leads to the same Q dependence of their intensities. The calculated intensity behavior based on eq 4 is compared with the experimental behavior for transitions I and II in Figure 3. The agreement nicely confirms the nature of the involved spin functions.

Magnetic Transitions from the Ground Spin Multiplet to the Excited Spin Multiplets. According to the $\Delta S = \pm 1$ selection rule, only transitions to the three excited $S = 3$ multiplets are expected to have appreciable intensity at low temperature (see Figure 9). The experimental bands V, VI, and VII in Figures 4 and 6 are thus assigned as $S = 4$ to $S = 3$ transitions. Each band is a convolution of several transitions, as the excited spin multiplets are also split into M components due to the single-ion anisotropies. The lower resolution of the spectrometer in this energy range prevents us from resolving the individual M components contributing to these bands. Nevertheless we can compare the total relative intensities of these bands with the calculated ones by taking into account only those transitions having intensities higher than 5% of the most intense one. A comparison of experimental and calculated values is given in Table 1, and the agreement is very good. Furthermore the theoretical Q dependence of band V in Figure 5 agrees with the experiment. The theory predicts a maximum in intensity around 1.0 \AA^{-1} , in good agreement with the experimental data. This feature is a fingerprint of a $\Delta S = \pm 1$ transition.

As we have seen before, within the $S = 4$ ground spin multiplet the energy splitting is related to the average value of D and D' (see eq 6). Thus, no information about the values of the individual ZFS parameters, D and D' , can be obtained. However, this kind of information can be extracted from the magnetic excitations toward the $S = 3$ spin multiplets, as the observed energy level splitting strongly depends on the relative values of D and D' . That allows us to obtain accurate values for these two parameters (the estimated error is lower than 5%).

Analysis of the Magnetic Measurements in the Light of the INS Results. To fit the magnetic properties the additional parameters of the model are the g components of each center. These can be derived from a fit of eq 1 supplemented by a Zeeman term to the susceptibility data, fixing the exchange parameters derived from INS in eq 2. The numerical procedure developed in the ref 22 has been used. A very good fit is obtained for an isotropic g value for all the $\text{Ni}(\text{II})$ centers, $g = 2.08$. Since we only measured magnetic data in powders, these were fit with a theoretical $\chi_{\text{powder}} = (\chi_{\parallel} + 2\chi_{\perp})/3$. The quality of the fit is excellent in the whole temperature range, as depicted in Figure 7. For comparison we have plotted in the same figure the behavior of a fully isotropic $\text{Ni}(\text{II})$ cluster neglecting the ZFS, and a significant difference between theory and experiment is seen in the low-temperature region.

With the parameters in eq 2 and $g = 2.08$, it has also been possible to reproduce the field dependence of the magnetization measured at 2 K. Due to the anisotropic nature of the system, an integration over all possible orientations of the magnetic field with respect to the uniaxial direction of the anisotropy was done in the calculation. As shown in Figure 8a the agreement is

excellent. For comparison, the behavior expected for an isotropic $S = 4$ spin state is also reported in the figure. As expected, it does not reproduce the observed behavior.

Indirect information concerning the zero-field splitting of the $S = 4$ ground state of the cluster can be obtained from the analysis of the temperature dependence of the magnetization at various fixed magnetic fields. On the basis of the exchange parameters derived from INS in eq 2 and $g = 2.08$, it is possible to obtain an excellent fit to the low-temperature behavior of the different magnetization curves. The calculated curves in Figure 8b were obtained with a value $\bar{D} = 0.543$ meV, in excellent agreement with the $\bar{D} = 0.535$ meV obtained from INS.

The excellent agreement of all the magnetic measurements with the corresponding curves calculated from the parameters derived from INS proves the physical relevance of the parameters in eq 2 and the formalism used in the treatment of the various interactions in this cluster.

Conclusions

The magnetic excitations observed by INS spectroscopy allowed us to determine the energy levels and wave functions of the low-lying spin states of the ferromagnetic Ni_4 cluster encapsulated in the polyoxometalate complex $[\text{Ni}_4(\text{H}_2\text{O})_2(\text{PW}_9\text{O}_{34})_2]^{10-}$. INS has shown that an isotropic Heisenberg model supplemented by a single-ion zero-field-splitting term is the appropriate Spin Hamiltonian for the description of the ground-state properties of this cluster. Complete and reliable information on both the magnetic exchange interactions and the spin anisotropy of the cluster has been derived for the first time, as the customarily used magnetic techniques have shown to be insufficient.

Thus, the bulk magnetic susceptibility provides information about the sign of the exchange interactions but has shown to be largely insensitive to their values, in particular to the pairwise interaction along the diagonal of the rhomb J' . In fact, satisfactory fits of the magnetic behavior can be obtained with J' ranging from 0 to 0.6 meV, while the interaction along the edges of the rhomb, J , remains within the range 0.78–0.88 meV. This insensitivity of the magnetic susceptibility to J' is a

consequence of the topology of the cluster, which leads to an energy spectrum where the energy gap between the ground spin level ($S = 4$) and the first excited one ($S = 3$) is equal to $4J$, independent of J' . The access to upper excited energy levels through INS has allowed us to get an accurate determination of this exchange parameter.

As far as the spin anisotropy of the cluster is concerned, we have shown that magnetization measurements provide indirect information on the splitting of the $S = 4$ ground spin state. Other techniques, such as high field EPR spectroscopy, can also be a valuable complement to get such splittings in a more direct way.²³ However, from these techniques it is almost impossible to extract any information on the splitting of the excited spin multiplets. Such information becomes essential in the present case, since this is the only way to distinguish between the two kinds of single-ion anisotropies present in the cluster as a consequence of the two different Ni(II) sites. Thus, the power of the INS technique becomes evident.

Finally, it is necessary to point out that this kind of study has been possible thanks to the great versatility of polyoxometalate chemistry in providing examples of largely insulated magnetic clusters of increasing nuclearities, definite topologies, and high symmetries with a variety of metal ions, which can be easily deuterated in big amounts. From a fundamental point of view, the INS study of these clusters in combination with other magnetic techniques should provide a unique opportunity to progress in the understanding of the magnetic exchange interaction phenomenon in polynuclear metal complexes, as well as in its parametrization using effective Hamiltonians.

Acknowledgment. This work has been developed in the framework of the European COST ACTION 518 (Project Magnetic Properties of Molecular and Polymeric Materials). Financial support by the Spanish Ministerio de Educación y Cultura (Grant PB96-0862) and the Swiss National Science Foundation are gratefully acknowledged. J.M.C.-J. thanks the Generalitat Valenciana for a predoctoral grant.

JA990197Z

(23) Barra, A. L.; Brunel, L. C.; Gatteschi, D.; Pardi, L.; Sessoli, R. *Acc. Chem. Res.* **1998**, *31*, 460.